Experimental study of H atom recombination on different surfaces in relation to H– negative ion production

S. Aleiferis, J. Bentounes, Stéphane Béchu, P. Svarnas, Alexandre Bés, Ana Lacoste, Lisseth Gavilan, J.L. Lemaire

Experimental study of H atom recombination on different surfaces in relation to H⁻ negative ion production

S. Aleiferis, J. Bentounes, S. Béchu, P. Svarnas, A. Bés, A. Lacoste, L. Gavilan, and J. L. Lemaire

View Online   **Export Citation**

ARTICLES YOU MAY BE INTERESTED IN

Detection of rovibrationally excited molecular hydrogen in the electronic ground state via synchrotron radiation
Applied Physics Letters **111**, 074103 (2017); https://doi.org/10.1063/1.4985617

Negative hydrogen ion production mechanisms
Applied Physics Reviews **2**, 021305 (2015); https://doi.org/10.1063/1.4921298

Surface recombination of hydrogen atoms studied by a pulsed plasma excitation technique
Journal of Applied Physics **89**, 2074 (2001); https://doi.org/10.1063/1.1325000

Experimental study of H atom recombination on different surfaces in relation to H⁻ negative ion production

S. Aleiferis[1,2,a)] J. Bentounes[1], S. Béchu[1,a)], P. Svarnas[2], A. Bés[1], A. Lacoste[1], L. Gavilan[3], J. L. Lemaire[4]

[1]*LPSC, Université Joseph Fourier Grenoble 1, CNRS/IN2P3, Grenoble INP, 53, Avenue des Martyrs, 38026, France*
[2]*High Voltage Laboratory, Electrical and Computer Engineering Department, University of Patras, 26504 Rion – Patras, Greece*
[3]*LATMOS, Université de Versailles Saint Quentin en Yvelines, 11 Bd d'Alembert 78280 Guyancourt, France*
[4]*LERMA, UMR 8112 du CNRS, de l'Observatoire de Paris et de l'Université de Cergy Pontoise, 5 mail Gay Lussac, F-95000 Cergy Pontoise Cedex, France*

[a)]Corresponding authors: aleiferis@ece.upatras.gr, stephane.bechu@lpsc.in2p3.fr

Abstract. Volume production of H⁻ negative ions is mostly attributed to the dissociative attachment of electrons to ro-vibrationally excited molecules. Apart from the main formation path for enriching the plasma with these molecules (i.e. radiative decay of singlet states excited by collisions with energetic electrons, EV excitation), an additional formation process refers to recombination of hydrogen atoms on the surface of materials which face the plasma. In this work, the importance of the later process is evaluated by considering various materials. Pyrex, Stainless Steel, Highly Oriented Pyrolytic Graphite (HOPG), and Yttrium, are sequentially tested in the ECR-driven H⁻ negative ion source ROSAE III. This source is specially designed to promote as much as possible surface recombination only on the surface of the specimen under test. Optical emission spectroscopy does prove a high degree of dissociation in this source. Furthermore, electron and negative ion densities are measured by means of electrostatic probe and laser photodetachment, respectively. The effectiveness of the above materials for the production of ro-vibrational states is thus evaluated indirectly, i.e. by comparing the values of the produced negative ion densities, assuming H⁻ production through DA mainly. The results suggest that, under the present conditions, the formation of ro-vibrational states is apparently dominated by process other than surface recombination.
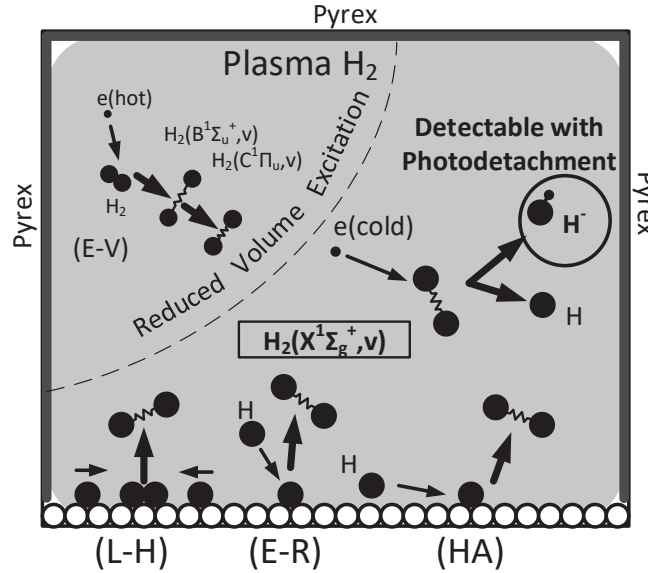
INTRODUCTION

The chamber walls of an ion source may have a catalytic effect on various elementary processes such as elastic scattering of particles, adsorption, vibrational deactivation, dissociative and associative mechanisms. Recombination of gas phase atoms is of particular importance in negative ion sources as it may recycle hydrogen atoms into vibrationally excited molecules.[1] By this way, the density of molecules vibrationally excited at levels necessary for enhanced dissociative attachment (DA) cross section [DA: $H_2(v) + e(cold) \rightarrow H_2^- \rightarrow H^- + H$] is increased and the density of the atoms which can destroy negative ions through detachment processes is reduced.

The catalyticity of the surface depends on the interaction of the gas phase species with the atoms on the crystal lattice of the surface and, on a bigger scale, the morphology of the surface. This catalyticity is quantified by the recombination coefficient γ which is defined as the ratio of the number of particles undergoing recombination to the total number of particles that flow onto the surface per unit time. Therefore γ assumes values from 0, for a non-catalytic, to 1, for a fully catalytic surface.[2]

Atom recombination mechanisms include Eley-Rideal (ER), Langmuir-Hinshelwood (LH), and hot-atom (HA) reactions. All of them require the earlier adsorption of an atom by the surface and lead to the formation of a molecule, which is then released (desorbed) back into the gas phase.

The above mechanisms may be quantified through a thermal macroscopic recombination coefficient. This coefficient, however, is the result of integration over the translational energy distribution of atoms and includes all the components that correspond to each ro-vibrational state. In order to study the effect of wall recombination on the vibrational kinetics, the state-specific recombination probability is needed.[3,4] Such studies have been realized for hydrogen at graphite and crystal metal surfaces, due to their relevance in plasma reactors for nuclear fusion[5,6] and interstellar chemistry[7,8]. For a more complete review on the phenomena involving hydrogen atom recombination on surfaces, the reader is referred to the work of Capitelli et al[2], and the references therein.

This work attempts to investigate how the recombinative desorption, leading to the formation of vibrationally excited molecules, may assist hydrogen negative ion (H⁻) production in ECR plasmas. In order to study the effect of various materials, the experiments should involve a practical sample size, i.e. small enough to reduce the cost. In this case, the issue is how to differentiate the vibrational states formed on the surface of the sample from those formed either on the chamber walls or in the volume of the plasma. To make this distinction, one of the formation paths needs to become dominant against the other(s). In the case of recombinative desorption studies, the volume production needs to be limited. This is the main concept of the present study, as depicted in Fig. 1. The goal is to reduce the vibrational excitation in the bulk of the plasma and on the surface of the chamber walls, and increase as much as possible the vibrational excitation on the surface of the material under test.

FIGURE 1. Concept of the source ROSAE III. The production of vibrationally excited molecules is limited as much as possible to the recombinative desorption on the surface of the material under test. L-H, E-R, and HA refer to the Langmuir-Hinshelwood, Eley-Rideal, and hot atom desorption mechanisms, respectively.

To clarify how this source configuration relatively amplifies vibrational heating through recombinative desorption on the surface of the material under test, the vibrational excitation mechanisms have to be discussed. Firstly, a simplified expression for the formation rate of vibrationally excited molecules in the volume of the plasma through EV excitation is given by the equation[9]:

$$\left.\frac{dn_v}{dt}\right|_{EV} = K_{EV}(T_{vib}, T_e) n_e n_{H_2} \tag{1}$$

where $K_{EV}(T_{vib},T_e)$ is an effective rate coefficient that accounts for the vibrational distribution, T_{vib} is an effective vibrational temperature, and T_e is the electron temperature. n_e is the density of electrons and n_{H_2} is the total density of molecules in their ground state. Secondly, the recombination rate of atoms on the chamber walls, is given by the equation[9] (terms before parenthesis):

$$\left.\frac{dn_v}{dt}\right|_{RD} = \frac{1}{4}n_H v_H \frac{A_{ch}\gamma_H}{V_{ch}} \left(= \frac{1}{4}n_H v_H \frac{A_{Py}\gamma_{H,Py} + A_s\gamma_{H,s}}{V_{ch}} \cong \frac{1}{4}n_H v_H \frac{A_s\gamma_{H,s}}{V_{ch}} \right) \tag{2}$$

where n_H is the density of atoms, v_H their thermal velocity, γ_H the probability of surface recombination on the chamber walls, A_{ch} is the total area of the chamber walls, and V_{ch} is the volume of the source. When two different materials are used for the interior of the chamber (here Pyrex and sample under test), as in the case of ROSAE III, the nominator $A_{ch}\gamma_H$ is replaced to account for the two different contributions (Eq. (2), terms in parenthesis). A_{Py} and $\gamma_{H,Py}$ refer to the surface area and the recombination coefficient of the Pyrex, and A_s and $\gamma_{H,s}$ refer to the surface area and the recombination coefficient of the sample under test.

Pyrex is a material (along with quartz) with a recombination coefficient that is greatly affected by the temperature.[10] By keeping the material below room temperature (water-cooled), the recombination coefficient is reduced to the order of 10^{-3}, while for typical plasma chamber temperatures (350-400 K) the recombination coefficient might be in the order of 10^{-2}. Metals like stainless steel have a recombination coefficient in the order of 10^{-1} or higher[11]. By covering the chamber walls with Pyrex, the surface production of vibrational states is limited to the surface of the material under test.

The ratio R_{EV}^{RD} related to the two sources of vibrational excitation, i.e. ratio of Eq. (2) to Eq. (1), is given by the expression:

$$R_{EV}^{RD} = \frac{dn_v/dt|_{RD}}{dn_v/dt|_{EV}} = \frac{n_H v_H}{4K_{EV}(T_{vib},T_e)n_e n_{H_2}} \frac{A_{ch}\gamma_H}{V_{ch}}$$

$$= \frac{n_H v_H}{4K_{EV}(T_{vib},T_e)n_e n_{H_2}} \frac{A_{Py}\gamma_{H,Py} + A_s\gamma_{H,s}}{V_{ch}} = \frac{n_H v_H}{4K_{EV}(T_{vib},T_e)n_e n_{H_2}} \frac{A_s\gamma_{H,s}}{V_{ch}} \tag{3}$$

In ROSAE III, this ratio is increased in two different ways. Firstly, the volume of the plasma is kept as low as possible, when compared with relevant ECR sources.[12,13] Secondly, as a consequence of the low recombination coefficient of the chamber walls (Pyrex), the atomic hydrogen density is increased.

EXPERIMENTAL SETUP

The experimental setup of the source ROSAE III is presented in Fig. 2. The source is driven by a network of 4 dipolar ECR sources.[14] The power from a single microwave generator (up to 1.2 kW), is divided into four equal parts and supplied to the ECR sources which are cooled with continuous flow of water.

A copper tube is welded over the cylindrical stainless steel chamber of the source. Water flows in the tube to keep the temperature of the chamber wall to relatively low levels (bellow room temperature). The Pyrex that covers the internal surface of the chamber is 5 mm thick and in direct contact with the chamber in order to improve thermal contact. The internal height of Pyrex is 214 mm and its internal diameter is 152 mm. The pumping of the source is realized with a turbo-molecular pump (50 l/s) adapted at the bottom of the source and the base pressure is in the order of 10^{-6} Torr. The plasma is sustained in pure hydrogen in a pressure that is accurately monitored with a Baratron pressure transducer.

The source ROSAE III is equipped with electrostatic probe, laser photodetachment, and optical emission spectroscopy (UV-Visible) diagnostic techniques. Electrostatic probe measurements are realized with a commercial automated acquisition system (SmartProbe, Scientific Systems). The tip of the probe is an L-bent tungsten wire 0.35 mm in diameter and with a total length of 15 mm. It is positioned 90 mm below the mid-plane of the ECR sources. Electron densities and temperatures are obtained with a simple fitting procedure in the I–V curve of the probe[15], while Electron Energy Distribution Functions (EEDFs) are obtained from the second derivative of the probe curve[16].

For the photodetachment technique, a Q-switched Nd:YAG laser is used. For the decoupling of the AC photodetachment signal, the capacitive decoupling circuit, presented in Fig. 2, is designed.[17] An energy density of

75 mJ/cm^2 ensures electron detachment from all H$^-$ ions in the irradiated volume and a probe DC bias +15 V above plasma potential (about +10 V) ensures that all the photo-detached electrons are collected.
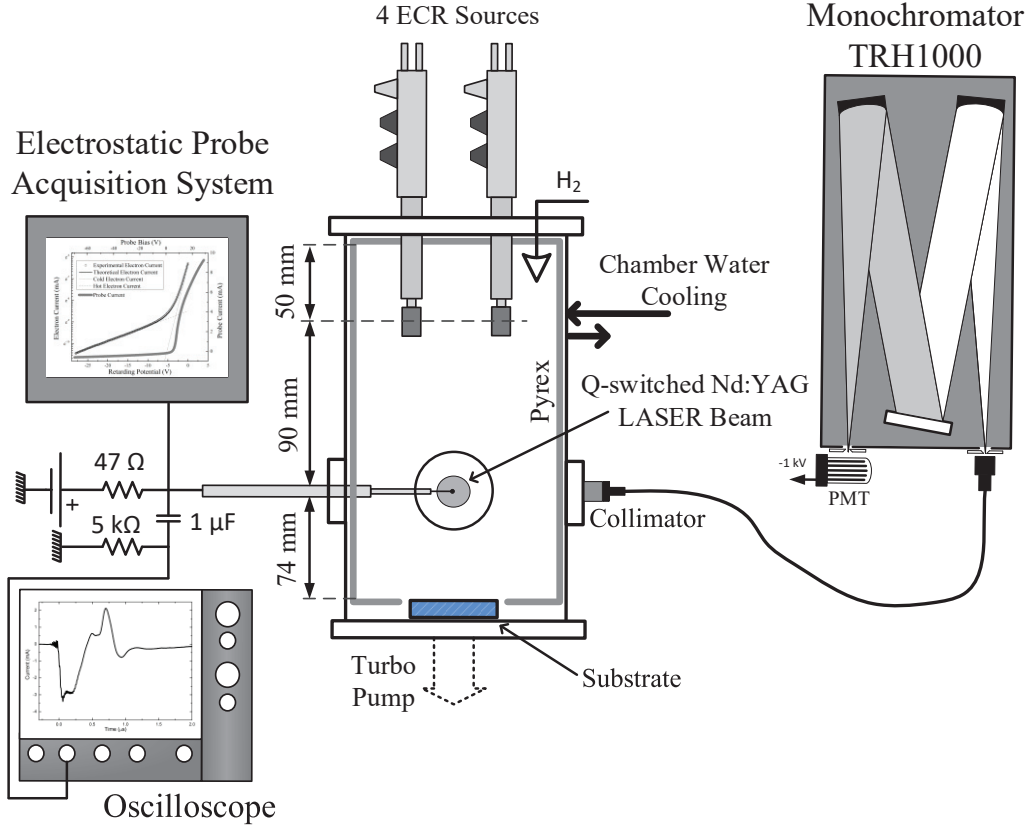

FIGURE 2. The source ROSAE III and the installed diagnostics.

Optical emission spectroscopy is carried out, at the same height with the probe measurements, with a monochromator (THR 1000) having 1 m focal length. Collimated light is led into the monochromator by an optical fiber. The spectroscopic system is calibrated in terms of relative spectral intensity with a quartz-tungsten-halogen lamp.

The spectroscopy is applied for the determination of the dissociation degree. The spectra in this case have to be interpreted by using a simple collisional-radiative model (also known as corona model) that was developed by Lavrov et al.[18] This model calculates the ratio of the first two atomic lines of Balmer series (H$_\alpha$ and H$_\beta$) to the Q1 line of the 2-2 band of the Fulcher-α band system (F(2-2)Q1). The central wavelengths of the H$_\alpha$, H$_\beta$, and F(2-2)Q1 lines in air are 656.283 nm, 486.134 nm, and 622.481 nm, respectively. The ratio of the atomic to the molecular line is given by the equation:

$$\frac{I_{\alpha,\beta}}{I_{F(2-2)Q1}} = \frac{1}{\eta\left(T_g\right)} \frac{\left(\left[H\right]/\left[H_2\right]\right)K_{dir}^{\alpha,\beta}\left(T_{tail}^{eff}\right) + K_{dis}^{\alpha,\beta}\left(T_{tail}^{eff}\right)}{A_{a21}^{d^-21}\tau_{d^-21}K_{ex}^{d^-21}\left(T_{tail}^{eff}\right)} \qquad (4)$$

where $\eta(T_g)$ is a function that reflects the dependence of F(2-2)Q1 line intensity on the molecular translational temperature, $[H]/[H_2]$ is the ratio of atomic to molecular density, $A_{a21}^{d^-21}$ is the probability of the $d^3\Pi_u^-,v=2,J=1 \rightarrow a^3\Sigma_g^+,v=2,J=1$ radiative transition, and τ_{d^-21} is the radiative lifetime of the $d^3\Pi_u^-,v=2,J=1$ state. $K_{dir}^{\alpha,\beta}$, $K_{dis}^{\alpha,\beta}$, and $K_{ex}^{d^-21}$ are the rate coefficients of the direct excitation of ground state atoms to the n=3 (α) and n=4 (β) electronic states, the dissociative excitation of ground molecules to the same states, and the excitation of ground

state molecules ($X^1\Sigma_g^+$,v=0,J=1) to the $d^3\Pi_u^-$,v=2,J=1 triplet state, respectively. These values have been reported as a function of the effective temperature of the high energy tail of the EEDF.[18] The degree of dissociation (D) is eventually calculated from the equation:

$$D = \frac{[H]}{[H]+2[H_2]} = \frac{[H]/[H_2]}{[H]/[H_2]+2} \tag{5}$$

RESULTS AND DISCUSSION

For the present study, five materials are chosen; i.e. Pyrex, stainless steel, Highly Oriented Pyrolytic Graphite (HOPG), tantalum, and yttrium. Pyrex is used as a control material since its surface recombination coefficient can be adjusted by temperature[10] and be kept in very low levels. Stainless Steel (SS) is very interesting as it is the most common chamber material. Tantalum has been mentioned as a material that can enhance negative ion production[19]. Finally, yttrium is a material with considerably lower work function (3.1 eV instead of ~4.5 eV for the other materials) which might affect the production in different ways (e.g. direct surface ionization).

The source ROSAE III is here operated at 5 mTorr of pure hydrogen and is supplied with 1 kW of microwave power, equally divided into the four ECR sources. A typical EEDF is presented in Fig. 3. The hot electron effective temperature, which is important for spectroscopy diagnostic, is practically the same for all the materials tested (i.e. 9.51 eV, 9.57 eV, 9.28 eV, and 9.45 eV for HOPG, SS, tantalum, and yttrium, respectively). The density of the hot electrons is in the order of 4×10^{-8} cm^{-3} for all the samples.
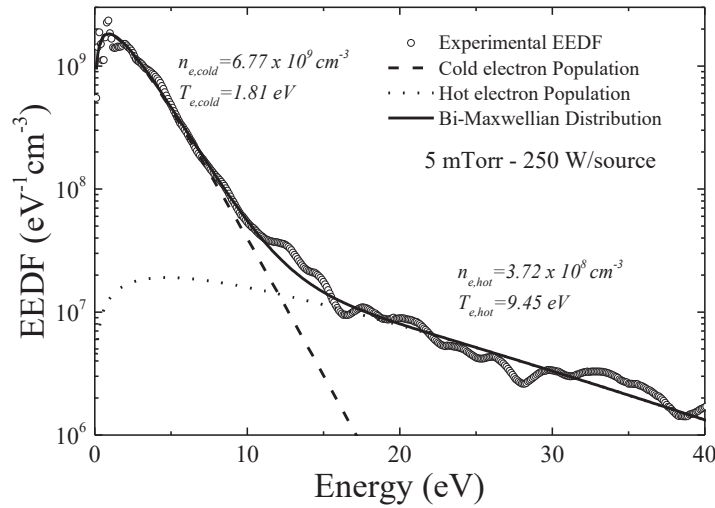
FIGURE 3. EEDF in the source ROSAE III when the internal surface of the chamber is covered with Pyrex. Power is 250 W/ECR source and pressure is 5 mTorr.

The temperature of the gas, can be determined from the rotational temperature which is measured from the Fulcher-α band. The diagnostic technique is described in detail by Iordanova.[20] Briefly, the rotational temperature is determined by the slop of the Boltzmann plot of $\ln\left(\lambda^4 I_{F\alpha22Q}/S_{J',J''}\right)$ versus $B_{v'}J'(J'+1)$, where λ is the emitted wavelength, $I_{F\alpha22Q}$ are the intensities of the lines of the 2-2Q band of the Fulcher-α system, $S_{J',J''}$ is the line strength, $B_{v'}$ is the rotational constant of the excited state, and J' is the rotational level.

The spectrum of the Fulcher-α band (as was measured under similar to the present experimental conditions) and the corresponding Boltzmann plot are both presented in Fig. 4. The estimated rotational temperature is 839 K. However, in low pressure plasmas, the translational and the rotational temperatures are not equal. According to Iordanova[20] the translational temperature is twice as high as the rotational one and, thus, in our case around 1700 K.
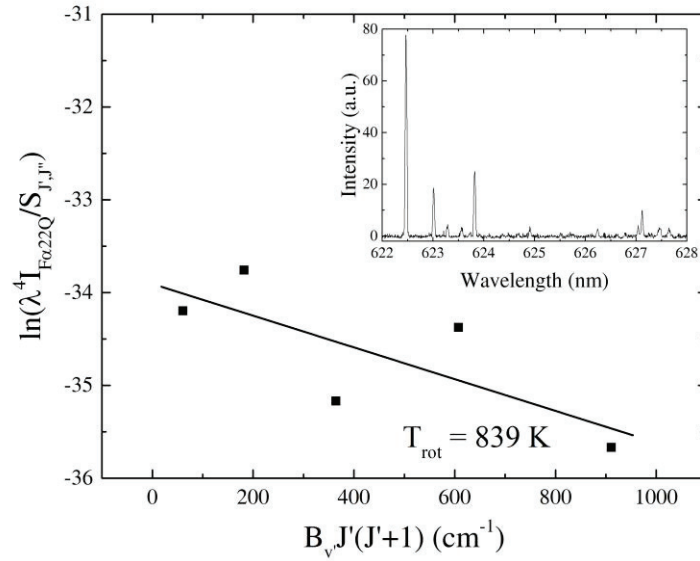
FIGURE 4. Boltzmann plot for the determination of the rotational temperature from the 2-2Q band of the Fulcher-α system. The inset presents the corresponding spectrum. This specific measurement has been realized previously under similar to the present experimental conditions.

The spectral lines used for the determination of the dissociation degree is presented in Fig. 5. The degree of dissociation, calculated here from the ratio between the Balmer-α line and the line of Fulcher-α band, is 57%, while the one calculated from the ratio between the Balmer-β line and the molecular line is 62%. These dissociation degrees correspond to n_H/n_{H2} ratios of 2.6 and 3.3, respectively. The used spectroscopic method becomes very sensitive to changes of the spectral line ratios when the density ratio n_H/n_{H2} becomes as high as the above values, which explains the difference between the two calculated degrees. Based on this result, the first requirement of this study, i.e. the presence of an important atomic density that can potentially recombine on the surface under test, is achieved.
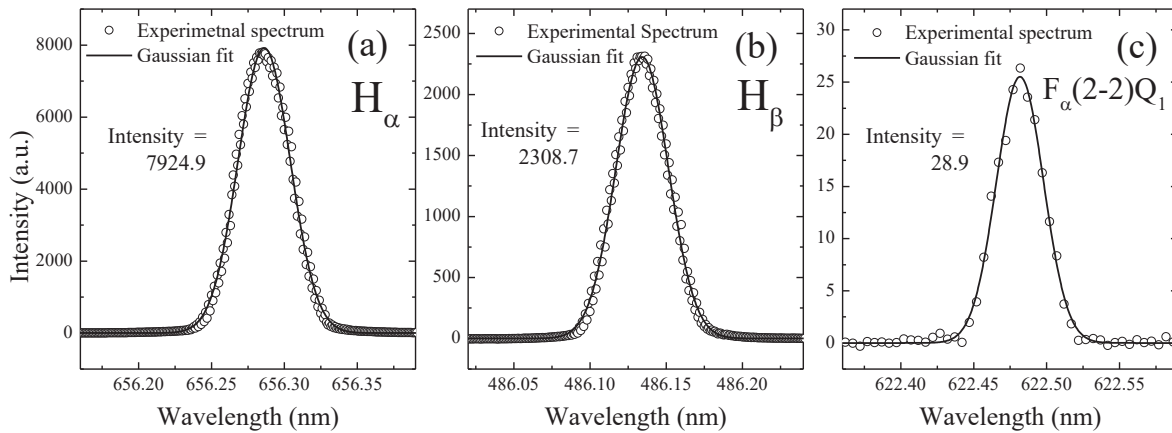
FIGURE 5. Spectral lines used for the determination of the degree of dissociation in ROSAE III.

The measured densities and temperatures of the cold electrons for different materials, are presented in Fig. 6. According to Fig. 6b, the electron temperature appears quite similar for all materials. According to Fig. 6a, the electron density for Pyrex, SS, HOPG, and tantalum, slightly varies in the range 6-7 x 10^9 cm^{-3}. On the contrary, the

electron density for yttrium rises at about 9×10^9 cm^{-3}, i.e. ~40% higher than the density observed for the rest materials, possibly due to the lower work function of yttrium.
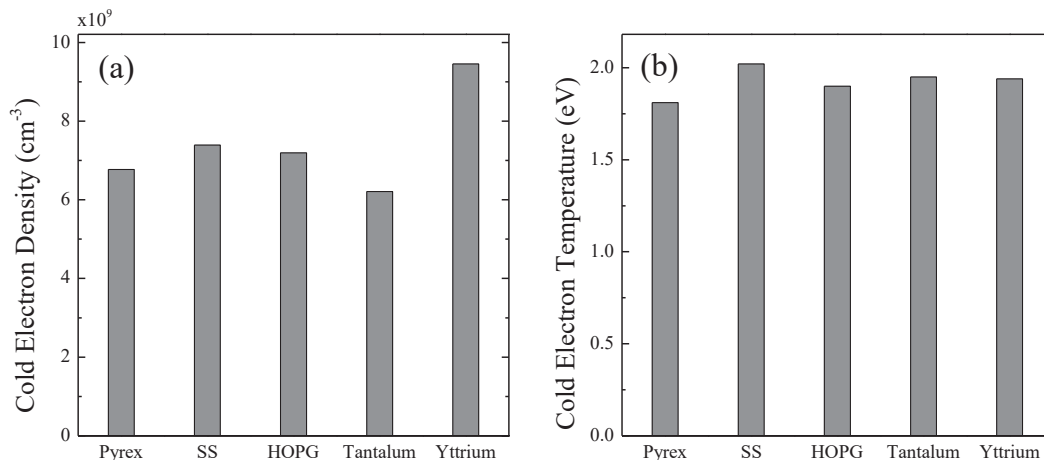
FIGURE 6. Cold electron (a) densities and (b) temperatures for the different materials tested here.

The negative ion densities and the n_{H-}/n_e ratios are presented in Fig. 7. According to Fig. 7a, SS and yttrium may be considered as better materials in terms of H$^-$ ion production (~70% increase in the case of yttrium), although one should keep in mind the tolerance of the photodetachment technique, i.e. around 20%.[21] Even if we attribute the observed increase in the absolute H$^-$ density to physical mechanisms, ignoring the measurement tolerance, Fig. 7b unveils a parallel increase in the electron density, since the n_{H-}/n_e ratios do not deviate as much as the H$^-$ densities for the different materials. Especially in the case of yttrium, this may happen due to the lower work function, which leads to secondary electron emission as mentioned above. Thus, any classification of the present materials in respect to the enhancement of the vibrationally excited molecules should be judicious.
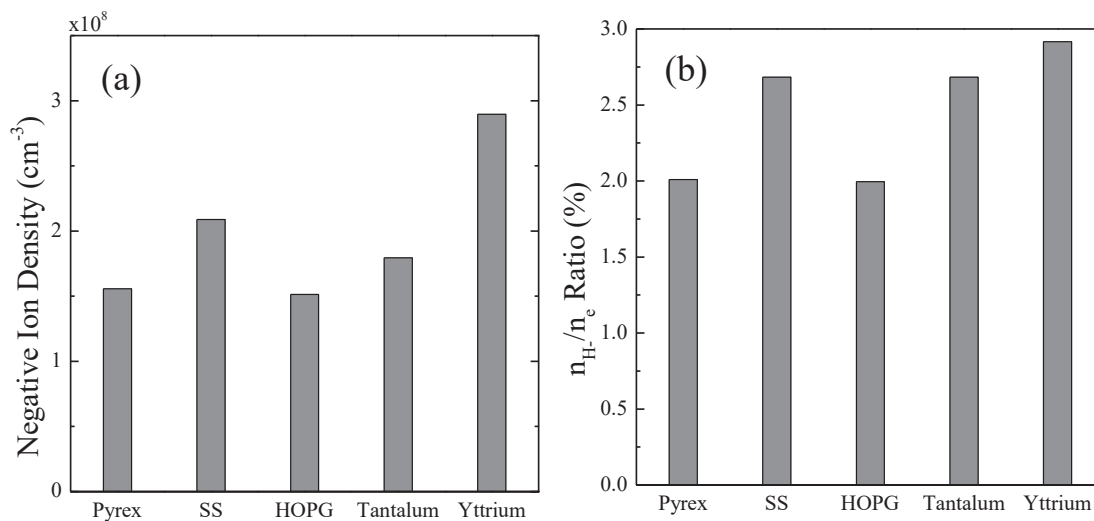
FIGURE 7. (a) Negative ion density and (b) n_{H-}/n_e ratio for the different materials tested here.

CONCLUSIONS

In the present work, five different materials were used in a specially designed H⁻ negative ion source for testing their efficiency in terms of recombinative desorption and subsequent formation of vibrationally excited molecules, which are a prerequisite for H⁻ production via dissociative attachment. High dissociation degrees were achieved, providing thus adequate precursors for recombinative desorption studies. To the extent that any variation of the negative ion density (as measured by means of photodetachment) mirrors changes of the vibrationally excited molecule densities (considering the dissociative attachment as dominant process for H⁻ production), stainless steel and yttrium appeared to be competitive materials for enhanced recombinative desorption. Despite that, for focusing better on the recombinative desorption mechanisms, variable parameters (e.g. the work function of each material) and further diagnostics, should be considered. Towards this direction, our group is currently studying the vibrational excitation of an unexcited (absence of plasma) atomic gas in contact with different surfaces, limiting hence the production of vibrational states solely to recombinative desorption. In this case, vibrationally excited molecules are probed by means of induced fluorescence and absorption diagnostics. However, these diagnostics are conducted in the VUV spectral range and synchrotron radiation facilities are used by our group in short scheduled periods. The results will thus be reported in due course.

ACKNOWLEDGMENTS

REFERENCES

[1] M. Bacal, Nucl. Fusion **46**, S250 (2006).

[2] Mario Capitelli, Roberto Celiberto, Gianpiero Colonna, Fabrizio Esposito, Claudine Gorse, Khaled Hassouni, Annarita Laricchiuta, Savino Longo, and Mario Capitelli, *Fundamental Aspects of Plasma Chemical Physics: Kinetics* (Springer, New York, 2016).

[3] G.D. Billing, Chem. Phys. **70**, 223 (1982).

[4] G.D. Billing, Comput. Phys. Rep. **12**, 383 (1990).

[5] I. Čadež, S. Markelj, Z. Rupnik, and P. Pelicon, J. Phys. Conf. Ser. **133**, 12029 (2008).

[6] M. Rutigliano and M. Cacciatore, Phys. Chem. Chem. Phys. **13**, 7475 (2011).

[7] E.R. Latimer, F. Islam, and S.D. Price, Chem. Phys. Lett. **455**, 174 (2008).

[8] J. Le Bourlot, F. Le Petit, C. Pinto, E. Roueff, and F. Roy, Astron. Astrophys. **541**, A76 (2012).

[9] D. Pagano, C. Gorse, and M. Capitelli, IEEE Trans. Plasma Sci. **35**, 1247 (2007).

[10] H. Wise and B.J. Wood, *Reactive collisions between gas and surface atoms* in *Advances in Atomic and Molecular Physics - Vol. 3*, edited by D.R. Bates and I. Estermann (Academic Press, 1967), p. 291.

[11] T. Mosbach, Plasma Sources Sci. Technol. **14**, 610 (2005).

[12] P. Svarnas, J. Breton, M. Bacal, and T. Mosbach, Rev. Sci. Instrum. **77**, 03A532 (2006).

[13] S. Aleiferis, P. Svarnas, I. Tsiroudis, S. Béchu, M. Bacal, and A. Lacoste, IEEE Trans. Plasma Sci. **42**, 2828 (2014).

[14] A. Lacoste, T. Lagarde, S. B chu, Y. Arnal, and J. Pelletier, Plasma Sources Sci. Technol. **11**, 407 (2002).

[15] N. Hershkowitz, *How Langmuir Probes Work* in *Plasma Diagnostics: Volume 1, Discharge Parameters and Chemistry*, edited by O. Auciello and D. Flamm (Academic Press, San Diego, 1989).

[16] V.A. Godyak and V.I. Demidov, J. Phys. D Appl. Phys. **44**, 269501 (2011).

[17] P.M. Bryant and J.W. Bradley, Plasma Sources Sci. Technol. **22**, 15014 (2013).

[18] B.P. Lavrov, N. Lang, A. V Pipa, and J. Röpcke, Plasma Sources Sci. Technol. **15**, 147 (2006).

[19] M. Bacal, A.A. Ivanov, M. Glass-Maujean, Y. Matsumoto, M. Nishiura, M. Sasao, and M. Wada, Rev. Sci. Instrum. **75**, 1699 (2004).

[20] S. Iordanova, J. Phys. Conf. Ser. **113**, 12005 (2008).

[21] S. Christ-Koch, U. Fantz, M. Berger, and NNBI Team, Plasma Sources Sci. Technol. **18**, 25003 (2009).